

Antiferroelectricity in ZrO_2 and Ferroelectricity in Zr, Al, La Doped HfO_2 Nanoparticles

A. T. Apostolov¹, I. N. Apostolova², J. M. Wesselinowa^{3*}

¹University of Architecture, Civil Engineering and Geodesy, Sofia, Bulgaria

²University of Forestry, Sofia, Bulgaria

³University of Sofia, Sofia, Bulgaria

Email: *julia@phys.uni-sofia.bg

How to cite this paper: Apostolov, A.T., Apostolova, I.N. and Wesselinowa, J.M. (2020) Antiferroelectricity in ZrO_2 and Ferroelectricity in Zr, Al, La Doped HfO_2 Nanoparticles. *Advances in Materials Physics and Chemistry*, **10**, 27-38.

<https://doi.org/10.4236/ampc.2020.102003>

Received: December 31, 2019

Accepted: February 18, 2020

Published: February 21, 2020

Copyright © 2020 by author(s) and Scientific Research Publishing Inc.

This work is licensed under the Creative Commons Attribution International License (CC BY 4.0).

<http://creativecommons.org/licenses/by/4.0/>



Open Access

Abstract

The dependence of the polarization P in $Hf_{1-x}Zr_xO_2$ nanoparticles on electric field, dopant concentration x , size and temperature are studied using the transverse Ising model and the Green's function method. Pure ZrO_2 shows at high electric fields an antiferroelectric behavior. Pure HfO_2 is a linear dielectric in the monoclinic phase. With increasing ZrO_2 content the $P(E)$ of HZO shows a ferroelectric behavior. The composition dependence x of the remanent polarization $P_r(x)$ has a maximum for $x = 0.5$. For $x = 0$, pure HfO_2 , and $x = 1$, pure ZrO_2 , $P_r = 0$. P increases with decreasing HZO nanoparticle size. The influence of Al and La doping on P_r in HfO_2 nanoparticles is also studied. The exhibiting of the ferroelectricity in ion doped HfO_2 is due to a phase transformation and to an internal strain effect. The observed results are in good qualitative agreement with the experimental data.

Keywords

ZrO_2 Nanoparticles, Zr, Al, La Doped HfO_2 Nanoparticles, Electric Properties, Microscopic Model, Green's Function

1. Introduction

ZrO_2 is a wide-band insulating material with a high dielectric constant. With increasing temperature in ZrO_2 exist monoclinic, tetragonal, orthorhombic and cubic phases. Antiferroelectric (AFE)-like double-hysteresis loops are observed in ZrO_2 thin films [1] [2] where the structure is tetragonal at room temperature [3] [4] [5] [6]. Using density functional calculations Reyes-Lillo *et al.* [7] have studied the experimentally reported field induced phase transition in ZrO_2 thin film [1] [2] which corresponds to an intrinsic effect.

Furthermore, ferroelectricity was found in HfO₂ thin films doped with Zr (HZO) [1] [4] [8] [9] [10] [11] [12] as well as with Si, Y, Al, Gd, La [13]-[20]. It must be noted that pure HfO₂ and ZrO₂ are not ferroelectric. HfO₂ exists with increasing temperature in monoclinic, tetragonal and cubic phases [21]. In nano-materials the tetragonal phase extends to lower temperatures [5]. For different Zr content x the HZO thin films show dielectric ($x = 0$), ferroelectric (for example $x = 0.5$) and AFE (for example $x = 0.7$) properties, which are due to the involvement of monoclinic (m-phase, P₂1/c-dielectric), orthorhombic (o-phase, Pca2₁-ferroelectric) and tetragonal (t-phase, P4₂/nmc-AFE) phases depending on the Hf:Zr ratio [1]. Wei *et al.* [9] reported that the polarization P in HZO increases with decreasing nanoparticle (NP) size. In HZO thin films P also increases significantly when the film thickness decreases [22].

Below a critical size of 30 nm pure ZrO₂ is stabilized in the tetragonal phase at room temperature which is considered as a crystallite size effect [23]. There are also reports for critical sizes for the tetragonal to monoclinic transformation between 15 - 20 nm [24] [25] [26]. The tetragonal phase of HfO₂ is stabilized for $d < 3.6 - 3.8$ nm [27].

The phase stability and the ferroelectricity of orthorhombic HZO ferroelectric material are theoretically investigated by Chen *et al.* [28] with density functional theory (DFT) computations. Oxygen defect impacts on ferroelectricity in HZO are studied using first-principles calculations by Wei *et al.* [29]. Also with the DFT Materlik *et al.* [30] have studied the ferroelectric phase of HfO₂, ZrO₂ and HZO. Batra *et al.* [31] revealed later that the results of Ref. [30] might not be correct. The experimentally observed stress in HZO films is tensile [32] whereas Batra *et al.* [31] reported a compressive stress.

The physical origin of the AFE hysteresis in ZrO₂ NPs and the ferroelectricity in HZO and Al, La doped HfO₂ NPs is still under debate. The aim of the present paper is to investigate theoretically these problems using a microscopic model and the Green's function technique.

2. Model and Green's Function

The properties of Zr doped HfO₂, Hf_{1-x}Zr_xO₂, NPs can be described by the transverse Ising model [33]:

$$H = -\sum_{i\alpha} \Omega_{\alpha} x_{i\alpha} S_{i\alpha}^x - \frac{1}{2} \sum_{ij\alpha\beta} J_{ij}^{\alpha\beta} x_{i\alpha} x_{j\beta} S_{i\alpha}^z S_{j\beta}^z - \mu E \sum_i S_{i\alpha}^z. \quad (1)$$

The pseudo-spin operator S_i^z characterizes the two positions of the ferroelectric unit at the lattice point i . J_{ij} is the pseudo-spin interaction between the pseudo-spins at sites i and j which is positive or negative in the ferroelectric or AFE case, respectively. The dynamics of the model with strength Ω is determined by the operator S^x . E is an external electric field. Here α, β mean Zr (or Al, La) or Hf. $x_i^{Zr} = 1$, $x_i^{Hf} = 0$ for pure ZrO₂, and $x_i^{Zr} = 0$, $x_i^{Hf} = 1$ for pure HfO₂. Thus, $x_i^{Zr} + x_i^{Hf} = 1$. Ω_{α} has two values— Ω^{Zr} and Ω^{Hf} . The interaction term $J_{ij}^{\alpha\beta}$ has three different values— J_{ij}^{Zr-Zr} , J_{ij}^{Hf-Hf} and J_{ij}^{Zr-Hf} .

The Hamiltonian (1) can be written in explicit form as ($x \equiv x^{Zr}$):

$$H = -\Omega^{Zr} \sum_i S_i^{xZr} x_i - \Omega^{Hf} \sum_i S_i^{xHf} (1-x_i) - \frac{1}{2} \sum_{ij} J_{ij}^{Zr-Zr} S_i^{zZr} S_j^{zZr} x_i x_j - \frac{1}{2} \sum_{ij} J_{ij}^{Hf-Hf} S_i^{zHf} S_j^{zHf} (1-x_i)(1-x_j) - \sum_{ij} J_{ij}^{Zr-Hf} S_i^{zZr} S_j^{zHf} x_i (1-x_j). \quad (2)$$

We assume that

$$\langle S_i^{zZr} x_i \rangle \approx \langle S_i^{zZr} \rangle x; \quad \langle S_i^{zHf} (1-x_i) \rangle \approx \langle S_i^{zHf} \rangle (1-x), \quad (3)$$

where $\langle x_i \rangle = x$. The factor x gives the concentration of the Zr ions which substitute the Hf ions, whereas $(1-x)$ is the concentration of the Hf ions.

The retarded Green's function is defined as:

$$G_{ij}(t) = -i\theta(t) \langle [B_i(t), B_j^+] \rangle. \quad (4)$$

The operator B_i stands for the set S_i^{+Zr} , S_i^{-Zr} , S_i^{+Hf} , S_i^{-Hf} , where S^- , S^+ are Pauli operators ($S = 1/2$, $S^z = S - S^- S^+$).

The polarization P of a HZO NP is obtained as:

$$P = \frac{1}{2N} \sum_n \tanh(\epsilon_n / k_B T). \quad (5)$$

The mixed transverse pseudo-spin-wave excitations ϵ_{ij} in a given shell n are calculated from the poles of the Green's function (4) using the method proposed by Tserkovnikov [34]:

$$\begin{aligned} \epsilon_{ij} &= \frac{1}{2} (\epsilon_{ij}^{11} + \epsilon_{ij}^{22}) \pm \sqrt{\frac{1}{4} (\epsilon_{ij}^{11} - \epsilon_{ij}^{22})^2 + \epsilon_{ij}^{12} \epsilon_{ij}^{21}}, \quad (6) \\ \epsilon_{ij}^{11} &= 2x\Omega^{Zr} \langle S_i^{-Zr} \rangle \delta_{ij} / \langle S_i^{zZr} \rangle \delta_{ij} - x(1-x) J_{ij}^{Zr-Hf} \langle S_i^{zHf} \rangle \\ &\quad - \frac{1}{2N'} \sum_m (1-x) J_{im}^{Hf-Hf} [2 \langle S_i^{zHf} \rangle - 4 \langle S_m^{zHf} S_i^{zHf} \rangle \delta_{ij} \\ &\quad + 2 \langle S_m^{-Hf} S_i^{+Hf} \rangle] / 2 \langle S_i^{zHf} \rangle \delta_{ij}, \\ \epsilon_{ij}^{22} &= 2(1-x)\Omega^{Hf} \langle S_i^{-Hf} \rangle \delta_{ij} / \langle S_i^{zHf} \rangle \delta_{ij} - x(1-x) J_{ij}^{Zr-Hf} \langle S_i^{zZr} \rangle \\ &\quad - \frac{1}{2N'} \sum_m x J_{im}^{Zr-Zr} [2 \langle S_i^{zZr} \rangle - 4 \langle S_m^{zZr} S_i^{zZr} \rangle \delta_{ij} \\ &\quad + 2 \langle S_m^{-Zr} S_i^{+Zr} \rangle] / 2 \langle S_i^{zZr} \rangle \delta_{ij}, \\ \epsilon_{ij}^{12} &= 2x\Omega^{Zr} \langle S_i^{+Zr} \rangle \delta_{ij} / \langle S_i^{zZr} \rangle \delta_{ij} \\ &\quad - \frac{1}{2N'} \sum_m x J_{im}^{Zr-Zr} \langle S_m^{+Zr} S_i^{+Zr} \rangle / \langle S_i^{zZr} \rangle \delta_{ij}, \\ \epsilon_{ij}^{21} &= 2(1-x)\Omega^{Hf} \langle S_i^{+Hf} \rangle \delta_{ij} / \langle S_i^{zHf} \rangle \delta_{ij} \\ &\quad - \frac{1}{2N'} \sum_m (1-x) J_{im}^{Hf-Hf} \langle S_m^{+Hf} S_i^{+Hf} \rangle / \langle S_i^{zHf} \rangle \delta_{ij}, \\ \langle S_i^{zZr} \rangle &= \frac{1}{2N'} \sum_j \frac{\epsilon_{ij}^{11}}{\epsilon_{ij}} \tanh \frac{\epsilon_{ij}}{2k_B T}, \end{aligned}$$

$$\begin{aligned}\langle S_i^{\text{Hf}} \rangle &= \frac{1}{4N'} \sum_j \frac{\epsilon_j^{22}}{\epsilon_j} \tanh \frac{\epsilon_j}{2k_B T}, \\ \langle S_i^{-\text{Zr}} \rangle &= \langle S_i^{+\text{Zr}} \rangle = \frac{1}{4} \frac{\epsilon_j^{12}}{\epsilon_j} \tanh \frac{\epsilon_j}{2k_B T}, \\ \langle S_i^{-\text{Hf}} \rangle &= \langle S_i^{+\text{Hf}} \rangle = \frac{1}{4} \frac{\epsilon_j^{21}}{\epsilon_j} \tanh \frac{\epsilon_j}{2k_B T},\end{aligned}$$

where N' is the number of lattice sites.

3. Numerical Results and Discussion

Our NP has an icosahedral symmetry. A certain Hf-spin is fixed in the center of the particle and all other spins are included into shells n . $n = 1$ denotes the central spin and $n = N$ represents the surface shell. Strain effects on the surface of the NP change the number of next neighbors on the surface and reduce the symmetry. Therefore the pseudo-spin interaction constants can take different values on the surface and in the bulk, denoted with the index “s” and “b”, respectively. Moreover, J is proportional to the inverse of the distance between two nearest spins, *i.e.* of the lattice parameters.

In order to clarify the AFE behavior in ZrO_2 we will firstly consider the electric field dependence of the polarization in the tetragonal phase of a ZrO_2 NP with $N = 3$ shells for $T = 300$ K. Materlik *et al.* [30] showed that AFE behavior of pure ZrO_2 thin films is observed after stabilization of the tetragonal phase for $d < 35$ nm. Using the lattice parameters for ZrO_2 from Ref. [30] in the tetragonal phase $a = 5.06$, $b = 5.18$, $c = 5.06$ (Å) we obtain the following model parameters: $J = -535$ K, $\Omega = 20$ K, $J_s = 1.6J_b$, $\Omega_s = 0.8\Omega_b$. The tetragonal structure is PbZrO_3 (PZO)-like AFE one, the electric dipoles are aligned antiparallel to their nearest neighbors—analogue to the magnetic moments in antiferromagnetic materials, therefore, we chose $J < 0$. The results are presented in **Figure 1**, curve 1. This AFE behaviour is in agreement with the experimental data of Ref. [2] [7] [30] [35] [36]. The polar AFE phase exists under a certain magnitude of the external electric field. When T increases, above a critical temperature T_{crit} only paraelectric properties can be observed. So, we can conclude, that one explanation of the origin of the AFE-ty in ZrO_2 NPs is a phase transformation from a tetragonal to an orthorhombic phase induced by an external electric field which is an intrinsic behavior. This is confirmed by the ab-initio study of Reyes-Lillo *et al.* [7].

Now we will study the electric behaviour for different electric field, temperature, crystal phase and size of $\text{Hf}_{1-x}\text{Zr}_x\text{O}_2$ NPs. By doping of ions with different radius appear different strains which give rise to additive changes (increasing or decreasing) of the pseudo-spin interaction constant $J_{ij} = J(r_i - r_j)$ in the defect sizes (denoted as J_d) compared to the undoped samples. The radius of the tetravalent Zr ion (86 pm) is a little larger than that of the Hf ion (85 pm), *i.e.* there is a small tensile strain ($J_d < J_b$), in agreement with the experimental data

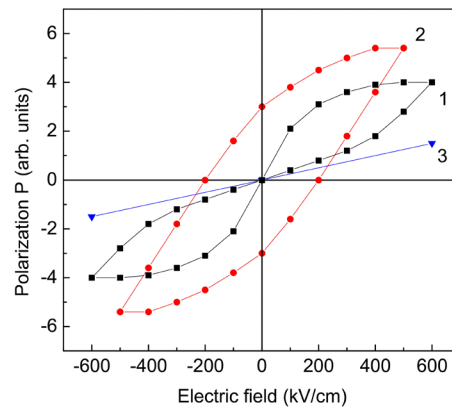


Figure 1. (Color online) Electric field dependence of the polarization in $\text{Hf}_{1-x}\text{Zr}_x\text{O}_2$ NPs for $N = 3$ shells, $J_s = 1.6J_b$, $\Omega_s = 0.8\Omega_b$ and different x values: (1) 1; (2) 0.5; (3) 0.

of Shiraishi *et al.* [32] for HZO thin films, whereas Batra *et al.* [31] reported a compressive stress.

The electric field dependence of the polarization in $\text{Hf}_{0.5}\text{Zr}_{0.5}\text{O}_2$ NPs is shown in **Figure 1**, curves 1-3. ZrO_2 and HfO_2 have almost equivalent crystal phases, with almost identical lattice parameters. It is seen that pure HfO_2 (**Figure 1**, curve 3) in the monoclinic phase is a linear dielectric with no notable nonlinear response of the polarization curve. As the ZrO_2 content increases, the $P(E)$ curve reaches its maximum value for doping concentration $x = 0.5$ (**Figure 1**, curve 2). ZrO_2 displays an AFE-behavior at high fields, where the polarization response becomes non-linear with hysteresis (**Figure 1**, curve 1). In the non-polar state where the polarization $P = 0$ we obtain a linear dependence in the polarization $P(E)$ below the Curie-Weiss temperature T_0 (curve 1). Above T_0 with increasing temperature, when the temperature is between T_0 and T_C (the ferroelectric phase transition Curie temperature), $T_0 < T < T_C$, there is a polar state, and the hysteresis loop is similar to the ferroelectric one (curve 2, $x = 0.5$). In this temperature region the crystal is in the orthorhombic phase where the electric dipoles are aligned parallel to their nearest neighbors, *i.e.* $J > 0$. Using the lattice parameters for HZO from [30] $a = 5.06$, $b = 5.14$, $c = 5.27$ Å we have calculated the following model parameters: $J_d = 505$ K, $\Omega_d = 20$ K. We assume $J_s = 1.6J_b$, $\Omega_s = 0.8\Omega_b$. The begin of the polar ferroelectric state corresponds to the monoclinic to orthorhombic phase transformation ($J > 0$). A similar ferroelectric hysteresis curve is obtained also for $x = 0.4$. This ferroelectric behaviour of HZO nanostructures is reported in Ref. [1] [9] [10] [28] [35] [37] [38]. Above T_C in the temperature interval $T_C < T < T_1$ the polar phase becomes to be metastable. Because of this the hysteresis curve shows a ferroelectric behavior. For $T_1 < T < T_N$ (the AFE phase transition temperature), we observe the AFE-like state ($J < 0$) (**Figure 1**, curve 1), typical for pure ZrO_2 NP ($x = 1$), the crystal phase is tetragonal. The polar phase cannot be induced when the temperature T is around T_N even under an external electric

field. For temperatures higher than the AFE transition temperature T_N in the cubic phase remain only paraelectric properties. The monoclinic phase decreases with increasing the ZrO_2 content. It can be seen from **Figure 1** that the remanent polarization P_r is zero for pure HfO_2 and ZrO_2 . P_r reaches at doping concentration $x = 0.5$ its maximum value.

In **Figure 2** is shown the composition dependence x of the remanent polarization P_r in HZO NPs. For $x = 0$, for pure HfO_2 , $P_r = 0$. With increasing of x P_r increases, reaches at $x = 0.5$ its maximum value and then in pure ZrO_2 , $x = 1$, P_r is again zero. The experimentally reported maximum value of the remanent polarization P_r is in the interval $x = 0.5 - 0.6$ [1] [37] [38] [39]. Mueller *et al.* [1] have shown that for $x = 0.5$ the ferroelectric phase is stable between 100 - 400 K. In this temperature interval HZO thin films for $x = 0.7$ show a transition to a double-loop hysteresis, whereas pure ZrO_2 thin films remain in this double-loop hysteresis starting from low temperatures.

To completely explain the ferroelectric-phase stability in HZO NPs, we want to focus now on the size dependence of the polarization P in HZO NPs which is demonstrated in **Figure 3**. It must be noted, that the distance between the shells is $\approx 10 \text{ \AA}$, *i.e.* we consider NPs with $N = 2 - 10$, *i.e.* with size of 2 - 50 nm. It can be seen from **Figure 3** that P increases with decreasing NP size, *i.e.* the ferroelectric properties disappear in large NPs, thick films and bulk materials, in agreement with the experimental data [9] [18] [40] [41]. This behaviour shows that the m-phase (non-ferroelectric), which is absent or very rarely found in the smallest NPs, increases with increasing size whereas the ferroelectric rhombohedral phase is stabilized by the existing surface strain. To conclude, we show that strain can be used in very small NPs of HZO to induce a ferroelectric phase, with a large polarization P and remanent polarization P_r . Park *et al.* [18] reported also that the o-phase increases with decrease thickness in HZO film. Clima *et al.* [42] show that oxygen vacancies can reduce drastically the polarization reversal barriers.

Finally, we will consider the effect of different ion doping on the electric properties of HfO_2 NPs. Variations of Al and La doping concentration influences the crystallographic structure of the NP and therefore the polarization. The insertion of a 3+ (Al) or 4+ (La) cation in the HfO_2 lattice leads to the appearance of oxygen vacancies to keep the charge balance. The radius of the Al ion (67.5 pm) is smaller compared to the ionic radius of the Hf ion (85 pm) (*i.e.* in our model we have $J_d > J_b$). **Figure 4** shows the remanent polarization P_r of the HfO_2 NP as a function of the Al-concentration (**Figure 4**, curve 1). The P_r value increases firstly by increasing the Al concentration starting at $x \approx 0.01$. The maximum ferroelectric polarization is reached at $x = 0.03$ Al, followed by an AFE region between $x = 0.04 - 0.06$ Al. At higher Al-concentrations the doped HfO_2 NP behaves as a paraelectric material. Mueller *et al.* [16] showed that the ferroelectricity is related to the non-centrosymmetric orthorhombic phase which is stabilized at low Al doping concentration.

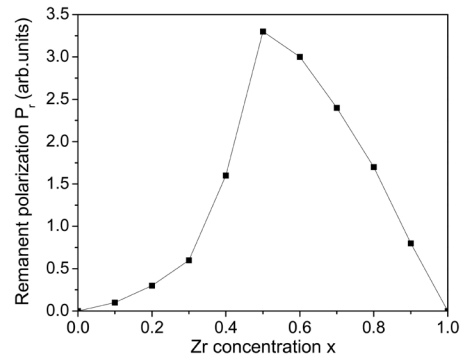


Figure 2. The remanent polarization of $\text{Hf}_{1-x}\text{Zr}_x\text{O}_2$ NPs for $J_s = 1.6J_b$, $\Omega_s = 0.8\Omega_b$, $J_d = 0.8J_b$, $\Omega_d = 1.2\Omega_b$, and different Zr concentration x .

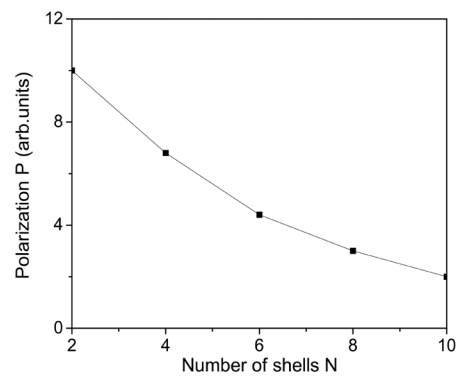


Figure 3. Size dependence of the polarization of HZO NPs for $J_s = 1.6J_b$, $\Omega_s = 0.8\Omega_b$.

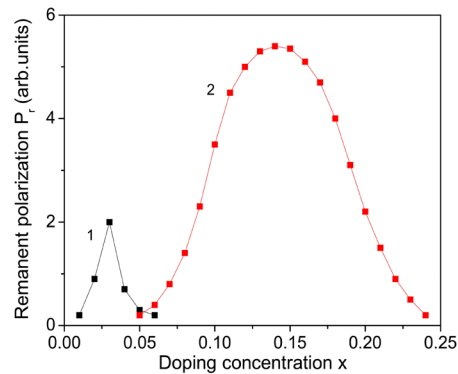


Figure 4. Doping concentration dependence of the remanent polarization P_r of a HfO_2 NP for doping with: (1) Al ($J_d = 605$ K); (2) La ($J_d = 451$ K) ions.

A similar behavior for the Al concentration dependence of the dielectric constant in HfO_2 thin films is reported by Yoo *et al.* [43].

The electric properties of La doped HfO_2 NPs are also studied. The radius of the La ion (117.2 pm) is larger compared to the ionic radius of Hf (85 pm) (this means $J_d < J_b$). Batra *et al.* [31] have shown that La doping stabilizes the or-

thorhombic phase. It can be seen from **Figure 4**, curve 2, that compared to the Al doping, the ferroelectric region for the La doped HfO₂ NP which starts at higher x value, $x \approx 0.05$, is shifted to higher doping concentrations and is broader due to the larger ionic radius of the La ion. In addition, the remanent polarization P_r is larger for the La doping than that for the Al doping (**Figure 4**, curves 2 and 1). The maximum value of P_r is observed for $x = 0.14$. Schroeder *et al.* [44] reported also that La shows the highest remanent polarization values of all ion doped HfO₂ thin films. Our results confirm the experimental data of Ref. [15] [44] for Al and La doped HfO₂ thin films. It must be noted that the observed here maximum values of the ion doped HfO₂ NPs are comparable to the values reported for Al-doped ($x = 0.025 - 0.03$ [43] [44] and for La-doped ($x = 0.12$ [16]) HfO₂ epitaxial thin films.

4. Conclusions

The properties of HZO are theoretically investigated till now with DFT computations. In this paper for the first time is used the microscopic transverse Ising model in order to clarify the physical origin of the AFE hysteresis in ZrO₂ NPs and the ferroelectricity in HZO and Al, La doped HfO₂ NPs which is still under debate. Therefore, we have investigated the dependence of the polarization P in ion doped HfO₂ NPs on electric field, dopant concentration x , size and temperature. Different from the DFT we study the behavior of the material at finite temperatures. To that aim we use a Green's function technique for $T \neq 0$. It can be concluded that the change in the polarization P_r with respect to the doping concentration in HfO₂ NPs is the result of the transformation of the crystalline phase due to the internal stress, of the appearance of an orthorhombic phase exhibiting ferroelectricity. Moreover, we try to clarify some discrepancies in the literature, for example about the appearing strain in HZO NPs (it is tensile and not compressible).

We obtain that pure ZrO₂ displays in the tetragonal phase an AFE-behavior ($J < 0$) at high fields inducing a t-o phase transformation. Pure HfO₂ is a linear dielectric in the monoclinic phase. With increasing the ZrO₂ content in HZO the hysteresis loop is consistent with that for ferroelectric materials ($J > 0$). $P_r(x)$ shows a maximum for $x = 0.5$. For $x = 0$ and $x = 1$ $P_r = 0$. It is shown that the properties of these three compounds—ZrO₂, HfO₂ and HZO—are changed with ion doping and size. The polarization P increases with decreasing NP size, *i.e.* the non-ferroelectric m-phase disappears with decreasing size. We show that strain can be used in very small NPs of HZO to induce a ferroelectric phase with large P and P_r .

The influence of Al and La doping on $P_r(x)$ in HfO₂ NPs is also studied. Stress due to the different ionic radii of the doping ions compared to the host ones (which cause different pseudo-spin interaction constants in the defect states) as well as the distribution of oxygen vacancies play a key role for the phase transformations in doped HfO₂ nanostructures. Both remanent polarizations

have a maximum value at $x \approx 0.03$ and 0.14 , respectively. The P_r curve for La doping is shifted to higher doping concentrations and is broader due to the larger radius of the La ion. Moreover, P_r is larger for La-doped compared with that of Al-doped HfO₂ NPs.

There are some differences in the electric properties of ion doped HfO₂ and ZrO₂ nanostructures [43] [45] [46]. For example Yoo *et al.* [43] observed that the dielectric constant in Al doped HfO₂ thin films undergoes a maximum whereas in Al doped ZrO₂ thin films it decreases. The electric properties of ion doped HZO and ZrO₂ NPs will be considered in the next paper.

Acknowledgements

One of us (A. A.) acknowledges financial support by the Bulgarian National Fund “Scientific Studies” (contract number KP-06-OPR 03/9).

Conflicts of Interest

The authors declare no conflicts of interest regarding the publication of this paper.

References

- [1] Mueller, J., Boescke, T.S., Schroeder, U., Mueller, S., Braeuhaus, D., Boettger, U., Frey, L. and Mikolajick, T. (2012) Ferroelectricity in Simple Binary ZrO₂ and HfO₂. *Nano Letters*, **12**, 4318-4323. <https://doi.org/10.1021/nl302049k>
- [2] Pestic, M., Hoffmann, M., Richter, C., Mikolajick, T. and Schroeder, U. (2016) Nonvolatile Random Access Memory and Energy Storage Based on Antiferroelectric Like Hysteresis in ZrO₂. *Advanced Functional Materials*, **26**, 7486-7494. <https://doi.org/10.1002/adfm.201603182>
- [3] Kim, S.K. and Hwang, C.S. (2008) Atomic Layer Deposition of ZrO₂ Thin Films with High Dielectric Constant on TiN Substrates. *Electrochemical Solid-State Letters*, **11**, G9-G11. <https://doi.org/10.1149/1.2825763>
- [4] Kim, H., McIntyre, P.C. and Saraswat, K.C. (2004) Microstructural Evolution of ZrO₂-HfO₂ Nanolaminate Structures Grown by Atomic Layer Deposition. *Journal of Materials Research*, **19**, 643-650. <https://doi.org/10.1557/jmr.2004.19.2.643>
- [5] Garvie, R.C. (1978) Stabilization of the Tetragonal Structure in Zirconia Microcrystals. *Journal of Physical Chemistry*, **82**, 218-224. <https://doi.org/10.1021/j100491a016>
- [6] Vollath, D., Fischer, F.D., Hagelstein, M. and Szabo, D.V. (2006) Phases and Phase Transformations in Nanocrystalline ZrO₂. *Journal of Nanoparticle Research*, **8**, 1003-1016. <https://doi.org/10.1007/s11051-006-9116-3>
- [7] Reyes-Lillo, S.E., Garrity, K.F. and Rabe, K.M. (2014) Antiferroelectricity in Thin-Film ZrO₂ from First Principles. *Physical Review B*, **90**, 140103(R). <https://doi.org/10.1103/PhysRevB.90.140103>
- [8] Lyu, J., Fina, I., Bachelet, R., Saint-Girons, G., Estanda, S., Gazquez, J., Fontcuberta, J. and Sanchez, F. (2019) Enhanced Ferroelectricity in Epitaxial Hf_{0.5}Zr_{0.5}O₂ Thin Films Integrated with Si(001) Using SrTiO₃ Templates. *Applied Physics Letters*, **114**, Article ID: 222901. <https://doi.org/10.1063/1.5096002>
- [9] Wei, Y., Nukala, P., Salverda, M., Matzen, S., Zhao, H.J., Momand, J., Everhardt, A.,

- Blake, G.R., Lecoer, P., Kooi, L.J., Iniguez, J., Dkhil, L. and Noheda, L. (2018) A Rhombohedral Ferroelectric Phase in Epitaxially Strained $\text{Hf}_{0.5}\text{Zr}_{0.5}\text{O}_2$ Thin Films. *Nature Materials*, **17**, 1095-1100. <https://doi.org/10.1038/s41563-018-0196-0>
- [10] Cheng, C.-K., Lin, M.-H., Chen, H.-Y., Fan, C.-C., Liu, C., Hsu, H.-H. and Chang, C.-Y. (2019) Impact of Zirconium Doping on Steep Subthreshold Switching of Negative Capacitance Hafnium Oxide Based Transistors. *Physica Status Solidi RRL*, **13**, Article ID: 1800573. <https://doi.org/10.1002/pssr.201800573>
- [11] Shibayama, S., Nishimura, T., Migita, S. and Toriumi, A. (2018) Thermodynamic Control of Ferroelectric-Phase Formation in $\text{Hf}_x\text{Zr}_{1-x}\text{O}_2$ and ZrO_2 . *Journal of Applied Physics*, **124**, Article ID: 184101. <https://doi.org/10.1063/1.5028181>
- [12] O'Connor, E., Halter, M., Eltes, F., Sousa, M., Kellock, A., Abel, S. and Fompeyrine, J. (2018) Stabilization of Ferroelectric $\text{Hf}_x\text{Zr}_{1-x}\text{O}_2$ Films Using a Millisecond Flash Lamp Annealing Technique. *APL Materials*, **6**, Article ID: 121103. <https://doi.org/10.1063/1.5060676>
- [13] Park, M.H., Schenk, T., Fancher, C.M., Grimley, E.D., Zhou, C., Richter, C., LeBeau, J.M., Jones, J.L., Mikolajick, T. and Schroeder, U. (2017) A Comprehensive Study on the Structural Evolution of HfO_2 Thin Films Doped with Various Dopants. *Journal of Materials Chemistry C*, **5**, 4677-4690. <https://doi.org/10.1039/C7TC01200D>
- [14] Boescke, T.S., Mueller, J., Braeuhaus, D., Schroeder, U. and Boettger, U. (2011) Ferroelectricity in Hafnium Oxide Thin Films. *Applied Physics Letters*, **99**, Article ID: 102903. <https://doi.org/10.1063/1.3634052>
- [15] Mueller, J., Schroeder, U., Boescke, T.S., Mueller, I., Boettger, U., Wilde, L., Sundqvist, J., Lemberger, M., Kuecher, P., Mikolajick, T. and Frey, L. (2011) Ferroelectricity in Yttrium-Doped Hafnium Oxide. *Journal of Applied Physics*, **110**, Article ID: 114113. <https://doi.org/10.1063/1.3667205>
- [16] Mueller, S., Mueller, J., Singh, A., Riedel, S., Sundqvist, J., Schroeder, J. and Mikolajick, T. (2012) Incipient Ferroelectricity in Al-Doped HfO_2 Thin Films. *Advanced Functional Materials*, **22**, 2412-2417. <https://doi.org/10.1002/adfm.201103119>
- [17] Kozodaev, M.G., Chernikova, A.G., Korostylev, E.V., Park, M.H., Khakimov, R.R., Hwang, C.S. and Markeev, A.M. (2019) Mitigating Wakeup Effect and Improving Endurance of Ferroelectric HfO_2 - ZrO_2 Thin Films by Careful La-Doping. *Journal of Applied Physics*, **125**, Article ID: 034101. <https://doi.org/10.1063/1.5050700>
- [18] Park, M.H., Lee, Y.H., Kim, H.J., Kim, Y.J., Moon, T., Kim, K.D., Mueller, J., Kersch, A., Schroeder, U., Mikolajick, T. and Hwang, C.S. (2015) Ferroelectricity and Antiferroelectricity of Doped Thin HfO_2 -Based Films. *Advanced Materials*, **27**, 1811-1831. <https://doi.org/10.1002/adma.201404531>
- [19] Dogan, M., Gong, N., Maae, T.-P. and Ismail-Beigi, S. (2019) Causes of Ferroelectricity in HfO_2 -Based Thin Films: An *Ab Initio* Perspective. *Physical Chemistry Chemical Physics*, **21**, 12150-12162. <https://doi.org/10.1039/C9CP01880H>
- [20] Schenk, T., Fancher, C.M., Park, M.H., Richter, C., Kuenneth, C., Kersch, A., Jones, J.L., Mikolajick, T. and Schroeder, U. (2019) On the Origin of the Large Remanent Polarization in La: HfO_2 . *Advanced Electronic Materials*, **5**, Article ID: 1900303. <https://doi.org/10.1002/aelm.201900303>
- [21] Wang, J., Li, H.P. and Stevens, R. (1992) Hafnia and Hafnia-Toughened Ceramics. *Journal of Materials Science*, **27**, 5397-5430. <https://doi.org/10.1007/BF00541601>
- [22] Park, M.H., Kim, H.J., Kim, Y.J., Lee, W. and Moon, T. (2013) Evolution of Phases and Ferroelectric Properties of Thin $\text{Hf}_{0.5}\text{Zr}_{0.5}\text{O}_2$ Films According to the Thickness and Annealing Temperature. *Applied Physics Letters*, **102**, Article ID: 242905.

- <https://doi.org/10.1063/1.4811483>
- [23] Tang, J., Zhang, F., Zoogman, P., Fabbri, J., Chan, S.-W., Zhu, Y., Brus, L.E. and Steigerwald, M.L. (2005) Martensitic Phase Transformation of Isolated HfO_2 , ZrO_2 and $\text{Hf}_x\text{Zr}_{1-x}\text{O}_2$ ($0 < x < 1$) Nanocrystals. *Advanced Functional Materials*, **15**, 1592-1602. <https://doi.org/10.1002/adfm.200500050>
- [24] Lu, C.-H., Raitano, J.-M., Khalid, S., Zhang, L. and Chan, S.-W. (2008) Cubic Phase Stabilization in Nanoparticles of Hafnia-Zirconia Oxides: Particle-Size and Annealing Environment Effects. *Journal of Applied Physics*, **103**, Article ID: 124303. <https://doi.org/10.1063/1.2936983>
- [25] Chraska, T., King, A.H. and Berndt, C.B. (2000) On the Size-Dependent Phase Transformation in Nanoparticulate Zirconia. *Materials Science and Engineering: A*, **286**, 169-178. [https://doi.org/10.1016/S0921-5093\(00\)00625-0](https://doi.org/10.1016/S0921-5093(00)00625-0)
- [26] Gou, G. and Chen, Y. (2005) A Nearly Pure Monoclinic Nanocrystalline Zirconia. *Journal of Solid State Chemistry*, **178**, 1675-1682. <https://doi.org/10.1016/j.jssc.2005.03.005>
- [27] Waetzig, G.R., Depner, S.W., Asayesh-Ardakani, H., Cultrara, N.D., Shahbazian-Yassarcd, R. and Banerjee, S. (2016) Stabilizing Metastable Tetragonal HfO_2 Using a Nonhydrolytic Solution-Phase Route: Ligand Exchange as a Means of Controlling Particle Size. *Chemical Science*, **7**, 4930-4939. <https://doi.org/10.1039/C6SC01601D>
- [28] Chen, P.-S. and Liu, C.W. (2019) Theoretical Calculation of Ferroelectric $\text{Hf}_{1-x}\text{Zr}_x\text{O}_2$ by First-Principle Molecular Dynamic Simulation. *Materials Research Express*, **6**, Article ID: 095045. <https://doi.org/10.1088/2053-1591/ab2cc2>
- [29] Wei, W., Ma, X., Wu, J., Wang, F., Zhan, X., Li, Y. and Chen, J. (2019) Spontaneous Polarization Enhancement in Ferroelectric $\text{Hf}_{0.5}\text{Zr}_{0.5}\text{O}_2$ Using Atomic Oxygen Defects Engineering: An *Ab Initio* Study. *Applied Physics Letters*, **115**, Article ID: 092905. <https://doi.org/10.1063/1.5115293>
- [30] Materlik, R., Kuennet, C. and Kersch, A. (2015) The Origin of Ferroelectricity in $\text{Hf}_{1-x}\text{Zr}_x\text{O}_2$: A Computational Investigation and a Surface Energy Model. *Journal of Applied Physics*, **117**, Article ID: 134109. <https://doi.org/10.1063/1.4916707>
- [31] Batra, R., Tran, H.D. and Ramprasad, R. (2016) Stabilization of Metastable Phases in Hafnia Owing to Surface Energy Effects. *Applied Physics Letters*, **108**, Article ID: 172902. <https://doi.org/10.1063/1.4947490>
- Batra, R., Huan, T.D., Jones, J.L., Rossetti Jr., G. and Ramprasad, R. (2017) Factors Favoring Ferroelectricity in Hafnia: A First-Principles Computational Study. *Journal of Physical Chemistry C*, **121**, 4139-4145. <https://doi.org/10.1021/acs.jpcc.6b11972>
- [32] Shiraishi, T., Katayama, K., Yokouchi, T., Shimizu, T., Oikawa, T., Sakata, O., Uchida, H., Imai, Y., Kiguchi, T., Konno, T.J. and Funakubo, H. (2016) Impact of Mechanical Stress on Ferroelectricity in $\text{Hf}_{0.5}\text{Zr}_{0.5}\text{O}_2$ Thin Films. *Applied Physics Letters*, **108**, Article ID: 262904. <https://doi.org/10.1063/1.4954942>
- [33] Pirc, R. and Blinc, R. (2004) Off-Center Ti Model of Barium Titanate. *Physical Review B*, **70**, Article ID: 134107. <https://doi.org/10.1103/PhysRevB.70.134107>
- [34] Tserkovnikov, Yu.A. (1971) Decoupling of Chains of Equations for Two-Time Green's Functions. *Theoretical and Mathematical Physics*, **7**, 511-519. <https://doi.org/10.1007/BF01028060>
- [35] Kim, S.J., Mohan, J., Lee, J.S., Kim, H.S., Lee, J., Young, C.D., Colombo, L., Sumnerfelt, S.R., San, T. and Kim, J. (2019) Stress-Induced Crystallization of Thin $\text{Hf}_{1-x}\text{Zr}_x\text{O}_2$ Films: The Origin of Enhanced Energy Density with Minimized Energy

- Loss for Lead-Free Electrostatic Energy Storage Applications. *ACS Applied Materials & Interfaces*, **11**, 5208-5214. <https://doi.org/10.1021/acsami.8b17211>
- [36] Peng, Y., Liu, Y., Han, G., Zhang, J. and Hao, Y. (2019) Germanium Negative Capacitance Field Effect Transistors: Impacts of Zr Composition in $\text{Hf}_{1-x}\text{Zr}_x\text{O}_2$. *Nanoscale Research Letters*, **14**, Article No. 125. <https://doi.org/10.1186/s11671-019-2927-9>
- [37] Park, M.H., Kim, H.J., Lee, Y.H., Kim, Y.J., Moon, T., Kim, K.D., Hyun, S.D. and Hwang, C.S. (2016) Two-Step Polarization Switching Mediated by a Nonpolar Intermediate Phase in $\text{Hf}_{0.4}\text{Zr}_{0.6}\text{O}_2$ Thin Films. *Nanoscale*, **8**, 13898-13907. <https://doi.org/10.1039/C5NR08346J>
- [38] Smith, S.W., Kitahara, A.R., Rodriguez, M.A., Henry, M.D., Brumbach, M.T. and Ihlefeld, J.F. (2017) Pyroelectric Response in Crystalline Hafnium Zirconium Oxide ($\text{Hf}_{1-x}\text{Zr}_x\text{O}_2$) Thin Films. *Applied Physics Letters*, **110**, Article ID: 072901. <https://doi.org/10.1063/1.4976519>
- [39] Zacharaki, C., Tsipas, P., Chaitoglou, S., Fragkos, S., Axiotis, M., Lagoyiannis, A., Negrea, R., Pintilie, L. and Dimoulas, A. (2019) Very Large Remanent Polarization in Ferroelectric $\text{Hf}_{1-x}\text{Zr}_x\text{O}_2$ Grown on Ge Substrates by Plasma Assisted Atomic Oxygen Deposition. *Applied Physics Letters*, **114**, Article ID: 112901. <https://doi.org/10.1063/1.5090036>
- [40] Kim, H.J., Park, M.H., Kim, Y.J., Lee, Y.H., Jeon, W., Gwon, T., Moon, T., Kim, K.D. and Hwang, C.S. (2014) Grain Size Engineering for Ferroelectric $\text{Hf}_{0.5}\text{Zr}_{0.5}\text{O}_2$ Films by an Insertion of Al_2O_3 Interlayer. *Applied Physics Letters*, **105**, Article ID: 192903. <https://doi.org/10.1063/1.4902072>
- [41] Onaya, T., Nabatame, T., Sawamoto, N., Ohi, A., Ikeda, N., Nagata, T. and Ogura, A. (2019) Improvement in Ferroelectricity of $\text{Hf}_x\text{Zr}_{1-x}\text{O}_2$ Thin Films Using Top- and Bottom- ZrO_2 Nucleation Layers. *APL Materials*, **7**, Article ID: 061107. <https://doi.org/10.1063/1.5096626>
- [42] Clima, S., McMitchell, S.R.C., Florent, K., Nyns, L., Popovici, M., Ronchi, N., Di Piazza, L., Van Houdt, J. and Pourtoiset, G. (2018) First-Principles Perspective on Poling Mechanisms and Ferroelectric/Antiferroelectric Behavior of $\text{Hf}_{1-x}\text{Zr}_x\text{O}_2$ for FEFET Applications. *IEEE International Electron Devices Meeting (IEDM)*, San Francisco, 1-5 December 2018, 16.5.1-16.5.4. <https://doi.org/10.1109/IEDM.2018.8614552>
- [43] Yoo, Y.W., Jeon, W., Lee, W., An, C.H., Kim, S.K. and Hwang, C.S. (2014) Structure and Electrical Properties of Al-Doped HfO_2 and ZrO_2 Films Grown via Atomic Layer Deposition on Mo Electrodes. *ACS Applied Materials Interfaces*, **6**, 22474-22482. <https://doi.org/10.1021/am506525s>
- [44] Schroeder, U., Richter, C., Park, M.H., Schenk, T., Pesic, M., Hoffmann, M., Fenger, F.P.G., Pohl, D., Rellinghaus, B., Zhou, C., Chung, C.C., Jones, J.L. and Mikolajick, T. (2018) Lanthanum-Doped Hafnium Oxide: A Robust Ferroelectric Material. *Inorganic Chemistry*, **57**, 2752-2765. <https://doi.org/10.1021/acs.inorgchem.7b03149>
- [45] Kozodaev, M.G., Chernikova, A.G., Khakimov, R.R., Park, M.H., Markeev, A.M. and Hwang, C.S. (2018) La-Doped $\text{Hf}_{0.5}\text{Zr}_{0.5}\text{O}_2$ Thin Films for High-Efficiency Electrostatic Supercapacitors. *Applied Physics Letters*, **113**, Article ID: 123902. <https://doi.org/10.1063/1.5045288>
- [46] Wang, Z., Gaskell, A.A., Dopita, M., Kriegner, D., Tasneem, N., Mack, J., Mukherjee, N., Karim, Z. and Khan, A.I. (2018) Antiferroelectricity in Lanthanum Doped Zirconia without Metallic Capping Layers and Post-Deposition/-Metallization Anneals. *Applied Physics Letters*, **112**, Article ID: 222902. <https://doi.org/10.1063/1.5037185>